PFC/JA 86-17

# Impurity Generation During ICRF Heating Experiments on Alcator C

H.L. Manning, J.L. Terry, B. Lipschultz,
B. LaBombard, B. D. Blackwell, C. L. Fiore
M.E. Foord, E.S. Marmar, J.D. Moody, R. R. Parker,
M. Porkolab, J.E. Rice

Plasma Fusion Center
Massachusetts Institute of Technology
Cambridge, MA 02139

August 1986

Submitted to NUCLEAR FUSION

This work was supported by the U.S. Department of Energy Contract No. DE-AC02-78ET51013. Reproduction, translation, publication, use and disposal, in whole or in part by or for the United States government is permitted.

# Impurity Generation During ICRF Heating Experiments on Alcator C

**H.L. Manning[1], J.L. Terry, B. Lipschultz, B. LaBombard[2], B.D. Blackwell[3], C.L. Fiore, M.E. Foord, E.S. Marmar, J.D. Moody, R.R. Parker, M. Porkolab, J.E. Rice**

**Plasma Fusion Center, Massachusetts Institute of Technology**
**Cambridge, Massachusetts, United States of America**

## Abstract

Observations of impurity behavior are presented from ICRF heating experiments at 180 MHz performed over a variety of conditions on the Alcator C tokamak, using graphite limiters and stainless steel antenna Faraday shields. Spectroscopic observations revealed significant increases in metal impurity concentrations during the RF pulse, with iron levels increasing by as much as a factor of 12 at the highest RF powers ($\sim$ 350–400 kW). Analysis of the inferred iron source rates shows an approximately linear dependence on RF power up to 400 kW, with no clear dependence on resonance conditions or bulk plasma parameters. However, a sharp increase in the temperature in the limiter shadow region was observed during the ICRF pulse, which was well correlated with the iron influx rate. It is concluded from this and other evidence that physical sputtering of the Faraday shield due to an elevated sheath potential is the primary source of metal impurities during ICRF heating on Alcator C. The same process, occurring at the graphite limiter, is believed to be the dominant source of carbon and oxygen. Calculated sputtering yields obtained from an edge erosion code demonstrate the plausibility of this model.

---

[1] Department of Physics, Harvard University, Cambridge, Massachusetts; now at Science Research Laboratory, Somerville, Massachusetts

[2] Now at UCLA School of Engineering and Applied Science, Los Angeles, California

[3] Now at Australian National University, Canberra

## 1. Introduction

Resonant heating of fusion plasmas via absorption of waves launched in the Ion Cyclotron Range of Frequencies (ICRF) has long been considered an attractive method of efficiently raising plasma temperatures to reactor levels [1]. As discussed below, early ICRF experiments on tokamaks were often plagued by large metallic impurity influxes which severely limited the amount of RF power that could be successfully delivered to the plasma and the temperature increases obtained. Although several recent experiments have studied and, to some extent, overcome this problem [2–7], there remains no clear consensus as to the principal source of metal impurities or the dominant mechanism for their release. Impurity generation during ICRF heating involves the complex interactions between the scrape-off layer (SOL) plasma, the RF fields, and the materials exposed to the SOL [8]: the limiter, the walls, and the ICRF antenna structure, which must be near the plasma to ensure good coupling. In order to extend ICRF heating to reactor level powers, further understanding of these interactions is needed to minimize the enhanced radiated power losses and impurity concentrations which persist in most of the current high power ICRF experiments.

On a high field, high density tokamak such as Alcator C, the high density plasma and limited port access render auxiliary heating via neutral beam injection (NBI) difficult. It is therefore especially important to understand the physics of RF heating on such devices. Impurity control is also vital, since the high electron densities involved lead to relatively high radiated power losses per impurity ion. This paper presents the first impurity measurements during ICRF heating experiments on the Alcator C Tokamak.

Early ICRF experiments at PLT, using stainless steel limiters, found the central iron concentration saturating at elevated but acceptable levels for 500 kW RF [9,10]. Since the installation of carbon limiters in 1980, metal impurity levels have dropped for ohmic (OH), RF, and NBI heated discharges, with radiated power now dominated by low Z (C,O) radiation from the peripheral plasma [2,11,12]. Metal impurity generation was further reduced through the use of carbon shields on the lateral faces of the metal antenna Faraday shields. However, both total radiated power ($\approx$ 30% $P_{RF}$) and metal impurity concentrations scaled linearly with RF power. PLT researchers concluded that the metal surfaces closest to the plasma contribute the most metal impurities, especially the Faraday shield ($\sim$ 3 cm outside the limiter radius), although the wall (10 cm outside the limiter radius) also contributes. The impurity influx appeared to be independent of ICRF heating mode or antenna poloidal extent.

ICRF experiments on TFR [3,13–19] used a graphite limiter and graphite "lateral

protections" on the antenna sides normal to the toroidal field to overcome an earlier dominance of central radiated power losses due to metals, yielding good heating results at $P_{RF} \leq 1.2$ MW. However, metal impurity radiation continued to scale linearly with $P_{RF}$ and was higher than for comparable OH and NBI powers. Results indicated that impurities generated from the antenna Faraday shield originated chiefly on the lateral surfaces (rather than the front surface facing the plasma) [3,19]. However, all metal surfaces in the SOL were judged to contribute to the metal influx, with no single dominant source. Metal impurity production in TFR was a non-local process attributed to changes in the SOL. This conclusion was supported by Langmuir probe measurements, in which the boundary electron density ($n_{eb}$ ) and temperature ($T_{eb}$ ) were observed to rise, with $T_{eb}$ proportional to $P_{\rm RF}$ up to 300 kW.

Increases of as much as 20-fold in radiated power due to the influx of metallic impurities also forced researchers at tokamak JFT-2 to abandon metal limiters and Faraday shields in favor of graphite limiters and TiC-coated shields [20,21]. Sputtering due to fast ions generated from some coupling of the ICRF power into the evanescent slow wave at the plasma edge was offered as a possible impurity generation mechanism by Kimura *et al.* [22]. More recently, researchers at the larger JFT-2M tokamak successfully applied up to 800 kW ICRF by utilizing graphite limiters and Ti Faraday shields [23,24]. Langmuir probes revealed a rise in the boundary electron temperature, $T_{eb}$, which was linear with respect to $P_{RF}$, and about twice as large as for similar NBI powers. It was concluded that sputtering of the limiter by ions accelerated through the sheath potential ($\Phi_{\rm sh} \approx 3T_{eb}$) was the dominant channel for the release of carbon and oxygen, but that some localized "additional mechanism" caused the Ti and Fe influx, only releasing iron from the walls near the antenna. It was suggested that sputtering via acceleration of both protons and multiply-charged low Z impurity ions by the strong reactive $\vec{E}_{\rm RF}$ fields generated near the antenna was the dominant source of metal impurities during these experiments.

ICRF heating experiments on the Nagoya tokamak, JIPP T-II [25], also encountered limitations due to metal impurity influx. Later results from the expanded JIPP T-IIU [26,27] showed that the brightness of line radiation from the limiter material (either steel or graphite) increased strongly as a function of $P_{RF}$. Probe measurements made at a radius between the Faraday shield and wall showed a linear increase with $P_{RF}$ of both $T_{eb}$ and $n_{eb}$ .

The common thread in all of these experiments is a significant change in the SOL, but the extent to which this perturbation is judged to be localized to the antenna region (fringing $\vec{E}_{\rm RF}$ field effects, loss of fast banana-trapped particles) or global (rise in $T_{eb}$, changes in $n_{eb}$, changes in recycling) seems to vary. Also, there is no clear agreement as

to the relative importance of direct coupling to electrostatic waves in the plasma edge, causing elevated $T_{eb}$ and/or fast ions, or of orbit or ripple losses of fast ions from the plasma core. It is likely that the various antenna designs, plasma edge characteristics, and choices of materials used in the above experiments have resulted in a variety of dominant impurity generation processes.

This paper presents impurity results from ICRF heating experiments at 180 MHz performed over a variety of conditions on the Alcator C Tokamak, using graphite limiters and stainless steel Faraday shields. Spectroscopic observations of impurity line radiation revealed large increases in metal impurity concentrations (Fe, Cr, Ni, Mo) during the RF pulse. Much smaller increases in carbon and oxygen were seen. Analysis of the inferred iron source rates shows an approximately linear dependence on RF power up to 400 kW, with no clear dependence on working gas (H or D), number of antennas used, or on resonance conditions (H 2nd harmonic, H minority in D, or off resonance). No correlation is observed with the presence of an ion tail or bulk ion heating. However, Langmuir probe data indicated a sharp increase in the temperature in the limiter shadow region during the ICRF pulse, well correlated with the iron influx rate. The behavior of carbon and iron during the highest power ICRF shots is in reasonable agreement with calculated sputtering yields of thermal ions (both hydrogen and impurity) striking, respectively, the graphite limiter at r = 12.5 cm and the Faraday shield at 13.2 cm. (The stainless steel wall is located at r = 19.2 cm.) This calculation uses the measured changes in the plasma edge temperature and density profiles.

Experimental details are presented in Section 2, with descriptions of Alcator C and the ICRF heating program, as well as diagnostics. The VUV spectrograph used to monitor impurities is described, and representative VUV spectra before and during ICRF heating are shown. Section 3 gives detailed information on the impurity influx. Impurity concentrations, $Z_{\rm eff}$ contributions, radiated power, and temporal behavior are presented. A one dimensional impurity transport code used to relate measured line brightnesses to derived quantities is described. The change in $Z_{\rm eff}$ during the RF pulse is shown to increase with increasing $P_{\rm RF}$ . Section 4 is concerned with the possible sources and release mechanisms responsible for the enhanced impurity influx. Results from surface analysis of the graphite limiter are presented, showing significant metal contamination. In order to compare the impurity influx with various plasma and RF parameters, data from many shots were compiled and analyzed. The edge source rate of iron (the dominant metal impurity) was selected as the variable best representing impurity generation. This quantity, $S_{\rm Fe}$, was deduced from measured iron line brightnesses through use of the transport code. Results of this survey and the correlations with edge probe measurements strongly suggest that physical sputter-

ing of both the limiters and Faraday shields through enhanced sheath potentials (due to elevated edge temperatures) is the primary cause of impurity release. Section 5 discusses the edge erosion code, the results of which are consistent with the above conclusion. A discussion of the Alcator C results and conclusions follows in section 6, with an attempt to place them in the context of the other tokamak ICRF experiments. Section 7 closes with a summary.

## 2. Experimental Details

This paper contains results from the first phase of the Alcator C ICRF heating program, conducted in 1984 [28,29]. Up to 400 kW of RF power at 180 MHz was delivered to the ICRF antenna, a full turn poloidal loop consisting of two pairs of half-turns which could be driven singly or together. The antenna Faraday shield was made of stainless steel and had an inner radius at r = 13.2 cm. Each half-loop was 4 cm wide in the toroidal direction. In these experiments, the ICRF power density at the antenna was as high as 1.4 kW/cm$^2$. However, the total ICRF input power never exceeded the Ohmic power. The target plasmas (a = 12.5 cm, R = 64 cm, $\overline{n_e}$ = 0.4–2.6$\times 10^{14}$ cm$^{-3}$, $I_P$ = 130–460 kA, $B_T$ = 6–12 T) had two graphite limiters separated toroidally by 180°. The antenna port was located 60° from the nearest limiter. ICRF power was launched in regimes of hydrogen second harmonic heating at $B_T \approx 6$ T, of hydrogen minority (0.5–3.0%) heating in a deuterium plasma at $B_T \approx 12$ T, and under non-resonant conditions ($B_T \approx$ 7–8 T in H, $B_T \approx$ 8–10 T in D). RF pulse lengths were typically 20–50 ms, ranging as high as 70 ms. Significant heating was obtained for the hydrogen minority regime, with a rise in $T_i$ of up to 500 eV at 400 kW RF (Figure 1). These highest power shots often underwent an electron density increase (typically from 1.2 to 1.9$\times 10^{14}$ cm$^{-3}$) as well as a rise in $Z_{\rm eff}$. (typically from 1.5 to 2.5–3.0). Heating results from the hydrogen second harmonic regime were ambiguous, with occasional rises in $T_i$ of up to 100 eV for $P_{\rm RF}$ up to 200 kW.

During the ICRF experiments, $T_e$ was measured from X-ray spectra and Thomson scattering, $n_e(r)$ was monitored by a 4-chord FIR laser interferometer, and $Z_{\rm eff}$ was deduced from visible bremsstrahlung emission. A neutral charge exchange (CX) analyzer measured $T_i$ and monitored fast ion tail formation. A single Langmuir probe with variable radial position was employed during some discharges to record the edge temperature and density profiles, $T_{eb}(r)$ and $n_{eb}(r)$. Soft X-ray emission (1–8 keV) was monitored by a PIN diode array with Be filters, while the X-ray PHA spectra (10–50 keV) were obtained with a $HgI_2$ detector.

A 2.2 meter grazing incidence time-resolving vacuum ultra-violet (VUV) spectrograph monitored impurity line radiation. The instrument was converted from a McPherson model

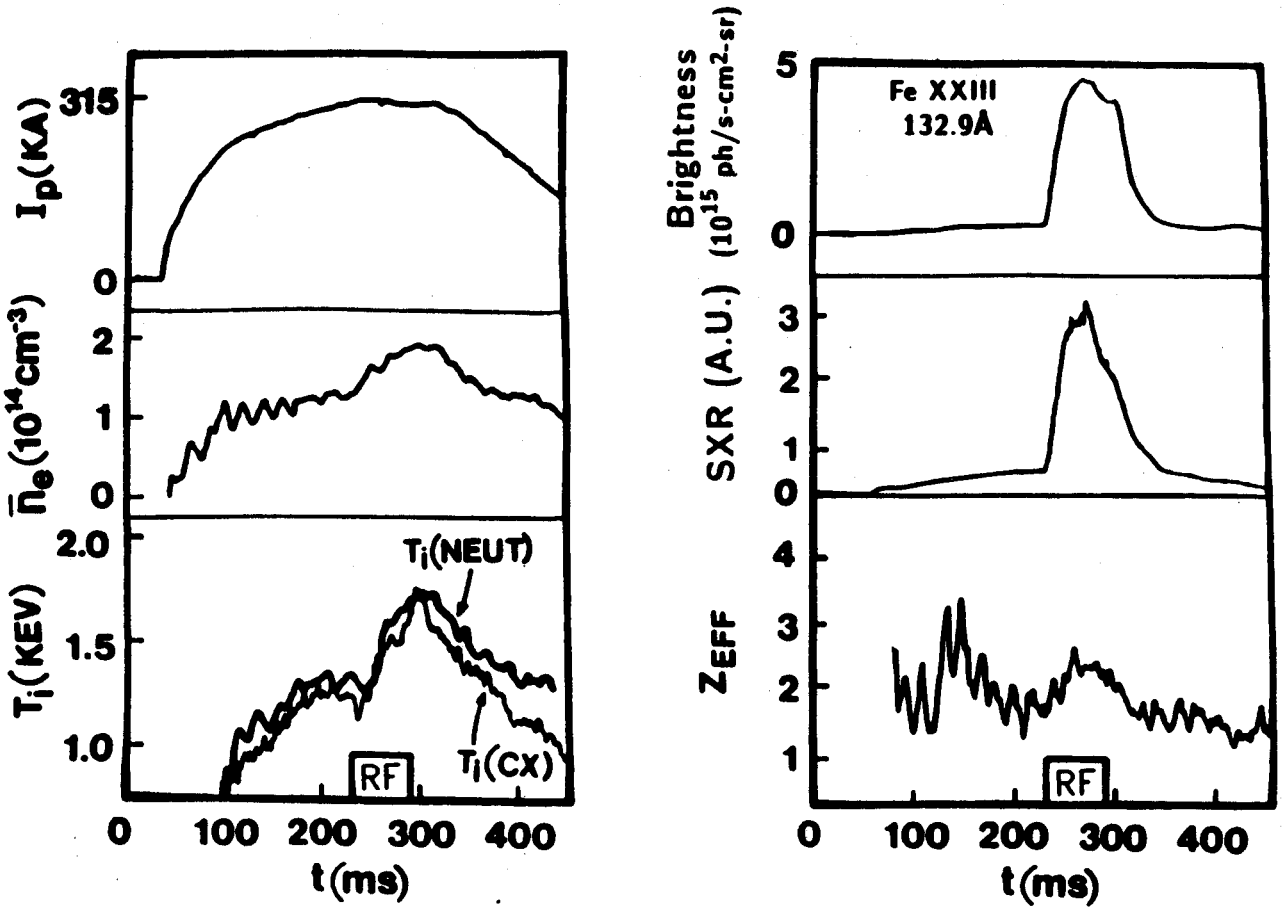


**Figure 1.** ICRF heating of H minority ions ($\sim$ 1.5–3.0%) in a D plasma. $P_{RF} \approx$ 380 kW. Shown are plasma current $I_P$, average density $\overline{n_e}$ , ion temperature of deuterium component $T_i$, brightness of Fe XXIII 132.87 Å resonance line (a central ionization state), soft X-ray emission (SXR, 1–8 KeV), and $Z_{eff}$. (The first four traces appeared in reference [28].)

247 monochromator by the installation of a detector similar to that described by Bell *et al.* [30] and others [31,32], consisting of a microchannel plate image intensifier which is coupled fiber-optically to a Reticon 1024-element linear photodiode array. When used with a 600 line/mm grating, the spectrograph has a spectral range of 20–1160 Å, with simultaneous coverage of $\sim$ 20 Å when centered at 30 Å and $\sim$ 100 Å when centered at 1100 Å. Spectral resolution is typically 0.3 Å FWHM at the lower wavelengths. The spectrograph sensitivity was absolutely calibrated [33] in the region 20–150 Å with a mini-focus e-beam soft X-ray source referenced to a proportional counter. Cross calibration at longer wavelengths was obtained through simultaneous comparisons of several impurity resonance lines with an absolutely calibrated monochromator on Alcator C. Neither the VUV spectrograph nor any of the other diagnostics was located at the toroidal position of the ICRF antenna.

## 3. Impurity Influx During ICRF Heating

The overall plasma cleanliness, as measured by $Z_{\rm eff}$ , deteriorated as $P_{\rm RF}$ was raised. The change in impurity content, $\Delta Z_{\rm eff}$ , is plotted versus $P_{\rm RF}$ in Figure 2, representing a wide variety of plasma conditions. Although there is a fair amount of scatter in the data, partially due to the variety of shots, $Z_{\rm eff}$ clearly increases with increasing $P_{\rm RF}$ . The trend is shown more clearly by the increase with $P_{\rm RF}$ of the iron source rate as derived from spectroscopic measurements (see below). There is no clear dependence of $\Delta Z_{\rm eff}$ on resonance conditions or working gas, although all of the points with $P_{\rm RF} > 250$ kW are from D plasmas with H minority. Pre-RF values of $Z_{\rm eff}$ ranged from 1.1 to 2.2.

Figure 3 shows a typical VUV spectrum before and during a 380 kW ICRF heating pulse. The large rise in metal impurity concentrations is exhibited by the brightness of the Fe XXIII resonance line, 132.87 Å, plotted versus time for the same discharge in Figure 1. The behavior of the C–VI line, on the other hand, reveals the relatively small increase in low-Z impurity levels during the ICRF pulse. Line brightnesses are obtained by fitting an instrumental response function to each viewed line, such that the summation of individual lines matches the observed spectrum.

The typical impurity content of the Alcator C plasmas before and during a series of 350–400 kW ICRF experiments in the hydrogen minority regime at $B_T \approx 12$ T was analyzed by comparing several measured line brightnesses from each major impurity element to those simulated by an impurity transport code. The transport code takes a given impurity source rate $S_z$ at the plasma edge and traces the evolution due to diffusion and atomic processes (ionization, radiative and dielectronic recombination, and excitation). Emissivity profiles and chordal brightnesses are calculated as a function of time for selected impurity

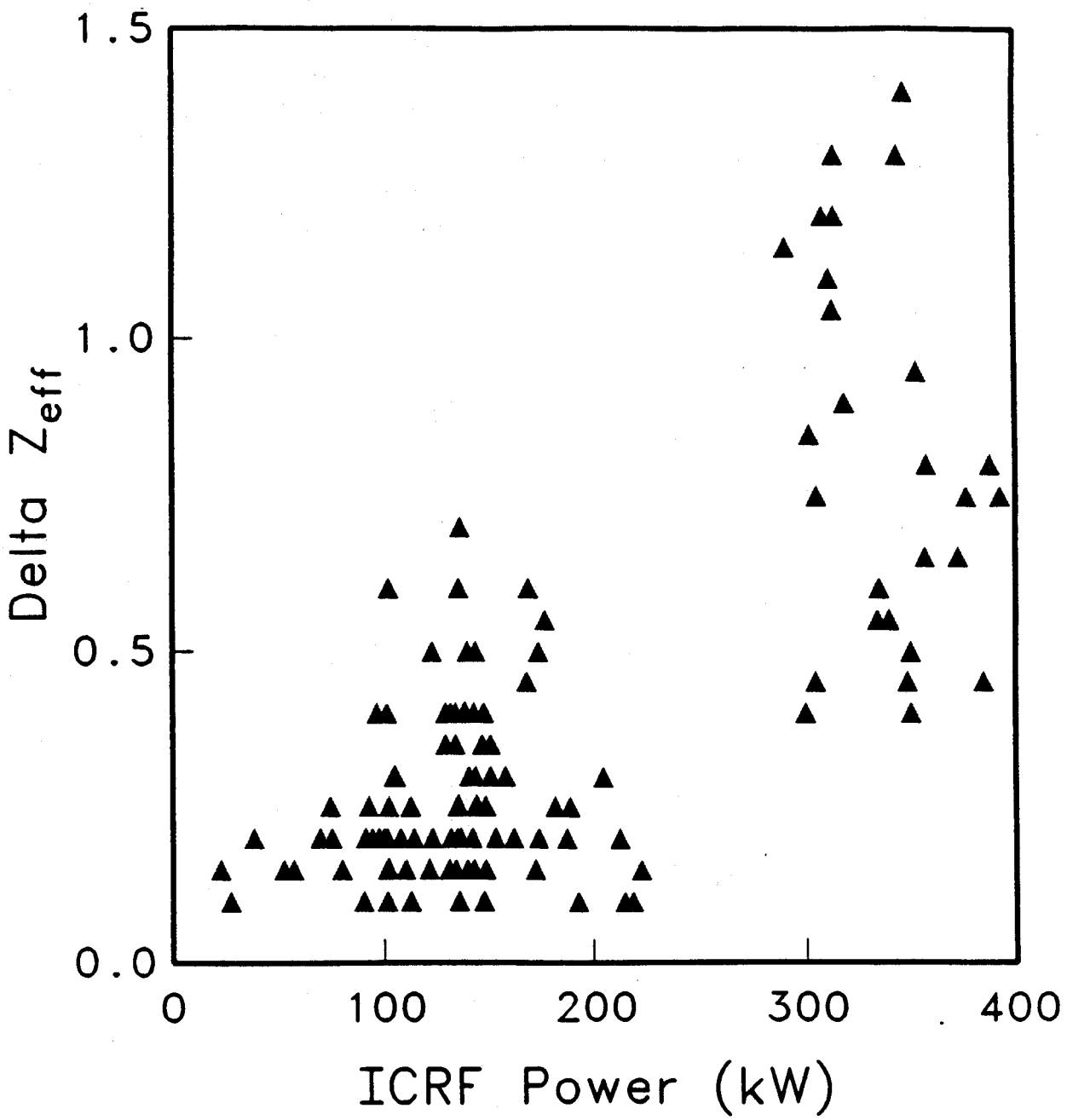


**Figure 2.** Change in $Z_{eff}$ during ICRF pulse vs. injected RF power.

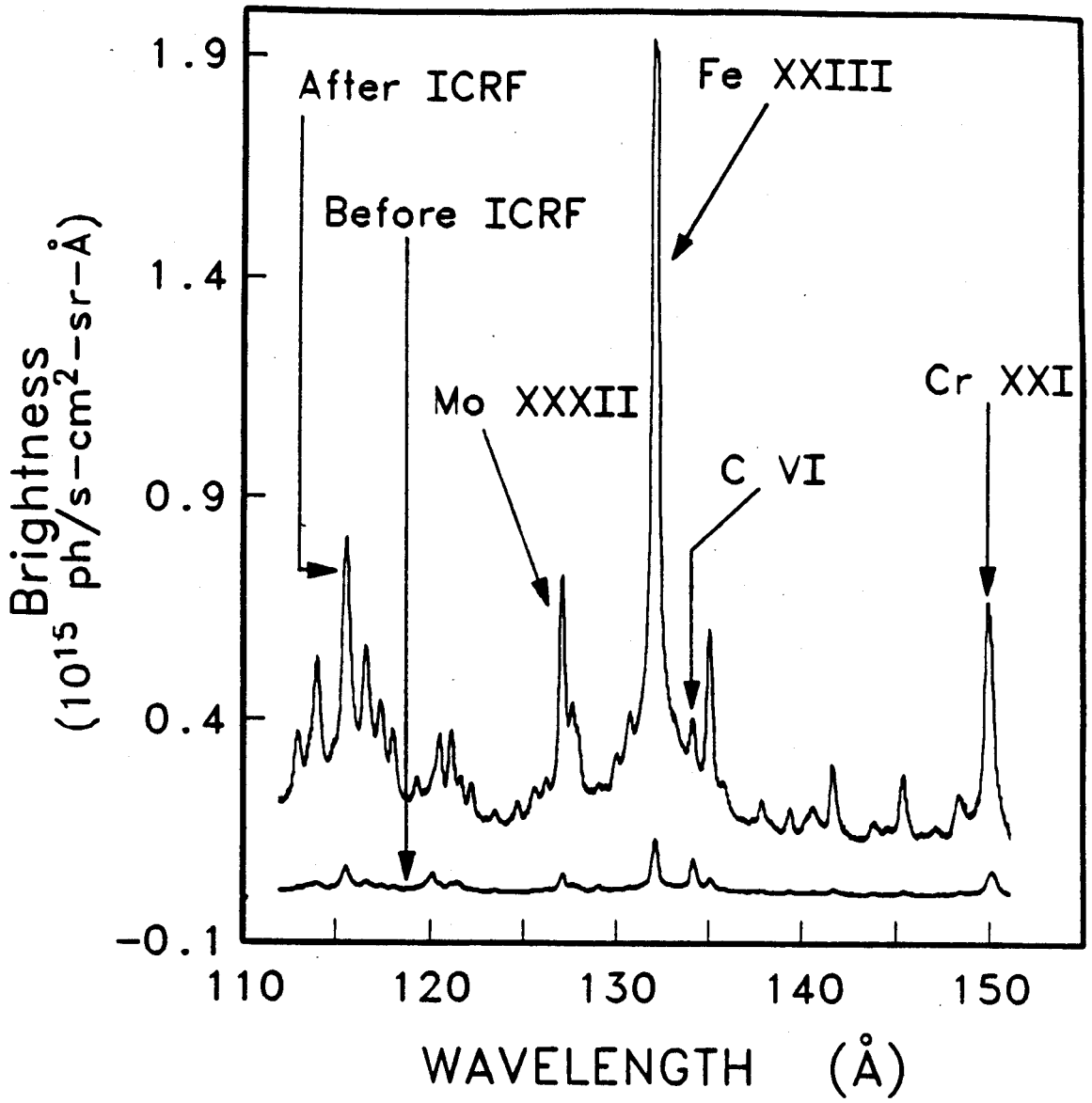


**Figure 3.** Evolution of VUV emission, 110–150 Å, during the discharge presented in Fig. 1, showing spectra taken before and just after the ICRF pulse. Impurity lines shown are Mo XXXII (127.81 Å), Fe XXIII (132.87 Å), C VI (134.94 Å and 33.74 Å in 4th order), and Cr XXI (149.90 Å). The Cr XXI line is blended with O VI (150.1 Å), which is dominant before the ICRF pulse.

ion lines. The transport model used is based on impurity confinement times measured by laser blow-off injection of trace impurities into purely ohmic discharges. Also using laser blow-off injection, similar transport was found in ICRF heated discharges. This lack of significant differences in impurity transport between ICRF heated and purely ohmic discharges was also reported on TFR, along with the conclusion that the capture of injected impurities from the scrape off layer to the region inside the limiter was unaffected by ICRF heating, despite measured perturbations to the SOL plasma during the ICRF pulse [34]. Anomalous spreading diffusion is used to simulate impurity transport, with the flux given by

$$\Gamma_j = -D\frac{\partial n_j}{\partial r} \tag{1}$$

where $n_j$ is the density of the j-th ionization state and $D$ is an empirically determined, spatially constant, impurity diffusion coefficient [35],

$$D(\mathrm{cm}^2/\mathrm{sec}) = 102\frac{a_l q_l (Z_{bg}/Z_{eff})}{m_{bg}} \tag{2}$$

where $a_l$ is the minor radius (cm), $q_l$ is the safety factor at the limiter, and $m_{bg}$ and $Z_{bg}$ are the mass and charge of the background gas in atomic units. Given the impurity transport, the plasma temperature and density profiles, and the measured impurity emission, the impurity concentration $n_z(r)$ and source rate $S_z$ are deduced.

Table I presents typical concentrations of the major impurities both before and just after 350–400 kW ICRF pulses in the minority heating regime. Calculated contributions to the central value of $Z_{\mathrm{eff}}$ are also given; the total agrees well with the measured values deduced from visible bremsstrahlung. The modest fractional increases in carbon and oxygen levels are dwarfed by the fractional increases in metallic impurities, especially iron and chromium (the main constituents of the stainless steel Faraday shield and walls). Iron supplants carbon as the dominant non-hydrogen component of $Z_{\mathrm{eff}}$ . The electron density rose typically 40% during these highest power RF pulses; but this increase is not fully due to the electrons from the increased impurity content. Total radiated power, estimated using densities determined here and the calculations of Post *et al.* [36], increased by an amount comparable to the injected RF power, with the largest increase due to iron. The fact that significant ion heating was observed during these shots ($\Delta T_i \approx 500$ eV, Figure 1), coupled with the observation that $T_e$ remained approximately constant at $\sim 2.1$ keV, indicates that this estimate of radiated power may be somewhat high. This is not surprising, as the estimated uncertainty in radiated power is at least a factor of two, due to uncertainties in impurity concentrations, assumptions of coronal equilibrium in Post *et al.*, and limited knowledge of edge plasma profiles, including probable asymmetries.

## Table I

### Impurity Concentrations* Before and After ICRF

350–400 kW, 50 msec pulse into D plasma with H minority

| | Pre-RF | End of RF |
|---|---|---|
| Central Impurity Densities ($cm^{-3}$) | | |
| Carbon | $3.1 \times 10^{12}$ | $3.6 \times 10^{12}$ |
| Oxygen | $1.6 \times 10^{11}$ | $3.0 \times 10^{11}$ |
| Chromium | $1.1 \times 10^{10}$ | $1.2 \times 10^{11}$ |
| Iron | $3.5 \times 10^{10}$ | $4.0 \times 10^{11}$ |
| Molybdenum | $1.7 \times 10^{9}$ | $1.2 \times 10^{10}$ |
| Central ($Z_{eff} - 1$) contributions | | |
| Carbon | 0.42 | 0.36 |
| Oxygen | 0.04 | 0.06 |
| Chromium | 0.02 | 0.24 |
| Iron | 0.09 | 0.70 |
| Molybdenum | 0.01 | 0.05 |
| Total | 0.58 | 1.41 |
| Total $Z_{eff}$ | 1.58 | 2.41 |
| Measured $Z_{eff}$ (vis. brems.) | 1.6 $\pm$0.2 | 2.4 $\pm$0.3 |
| Central Electron Density ($10^{14}cm^{-3}$) | 2.2 $\pm$ 0.4 | 3.0 $\pm$ 0.5 |
| Total Radiated Power (kW) | $\sim$ 30 | $\sim$350 |
| Input Power (kW): | | |
| Ohmic | $\sim$460 | $\sim$640 |
| ICRF | 0 | $\sim$350 |
| Total | $\sim$460 | $\sim$990 |

* Uncertainties in impurity concentrations are approximately $\pm$50%

The transport code predicts that the brightness of Fe IX (171 Å), an edge state, should closely track the Fe influx rate, $S_{Fe}$, so that a sudden increase in the brightness of this line implies that $S_{Fe}$ has increased to a new steady state value. Such behavior is indeed seen during a number of ICRF pulses (Figure 4), consistent with a rapid (2–5 ms) increase in $S_{Fe}$ coincident with the RF pulse. The temporal behavior of highly ionized Fe lines (e.g. Fe XXIII, Figure 1) is generally also in agreement with this model. It must be noted, however, that a more gradual rise in the Fe IX line is sometimes seen, perhaps indicative of a self-sputtering contribution with its inherent positive feedback.

4. Sources of ICRF Generated Impurities

Metal impurity ions can be liberated from edge structures by the following mechanisms [37]: arcing, evaporation, flaking or blistering, and sputtering due to neutrals, working gas ions, or impurity ions. Arcing within the antenna structure or between the antenna and wall is judged to be unimportant in these experiments because: 1) the iron influx appeared to be steady and reproducible during the RF pulse, unlike the erratic or intermittent behavior characteristic of such arcing; 2) no threshold value of $P_{RF}$ was seen; 3) no clear difference in impurity production was seen between the top half-loop and the bottom half-loop antennas; presumably eliminating arcing due to positioning errors; 4) the circuits driving the RF antennas shut down rapidly in the event of an arc detection, as manifested by sudden changes in the reflectivities. However, arcing may explain the few shots in which the iron level rose anomalously rapidly, leading to a disruption. A small melted spot found later at the base of one of the antenna sections is in fact attributed to arcing. The possibility of many small unipolar arcs between the antenna structure and the plasma sheath cannot be completely excluded. A steady production of such short-lived arcs, yielding neutral impurity atoms with energy in the 100 eV range [38], might produce the observed impurity influxes during ICRF heating. This phenomenon would be undetected by the arc detector or other diagnostics. However, visual inspection with a 10x-power eyepiece revealed no tiny pits or tracks, characteristic of such arcs, on the antenna or Faraday shield.

Flaking and blistering are also deemed unlikely due to their erratic nature. Evaporation is also considered an improbable explanation for the enhanced impurity influx during the ICRF pulse. The erosion code discussed below predicts a negligibly small contribution from this process, since the calculated heat load to the edge structures could only cause major evaporation if, for some reason, it were very localized. Furthermore, evaporative processes resulting from a constant flux of extra heat would have a steadily increasing yield as the temperature of the structures involved rises towards the melting point. The time

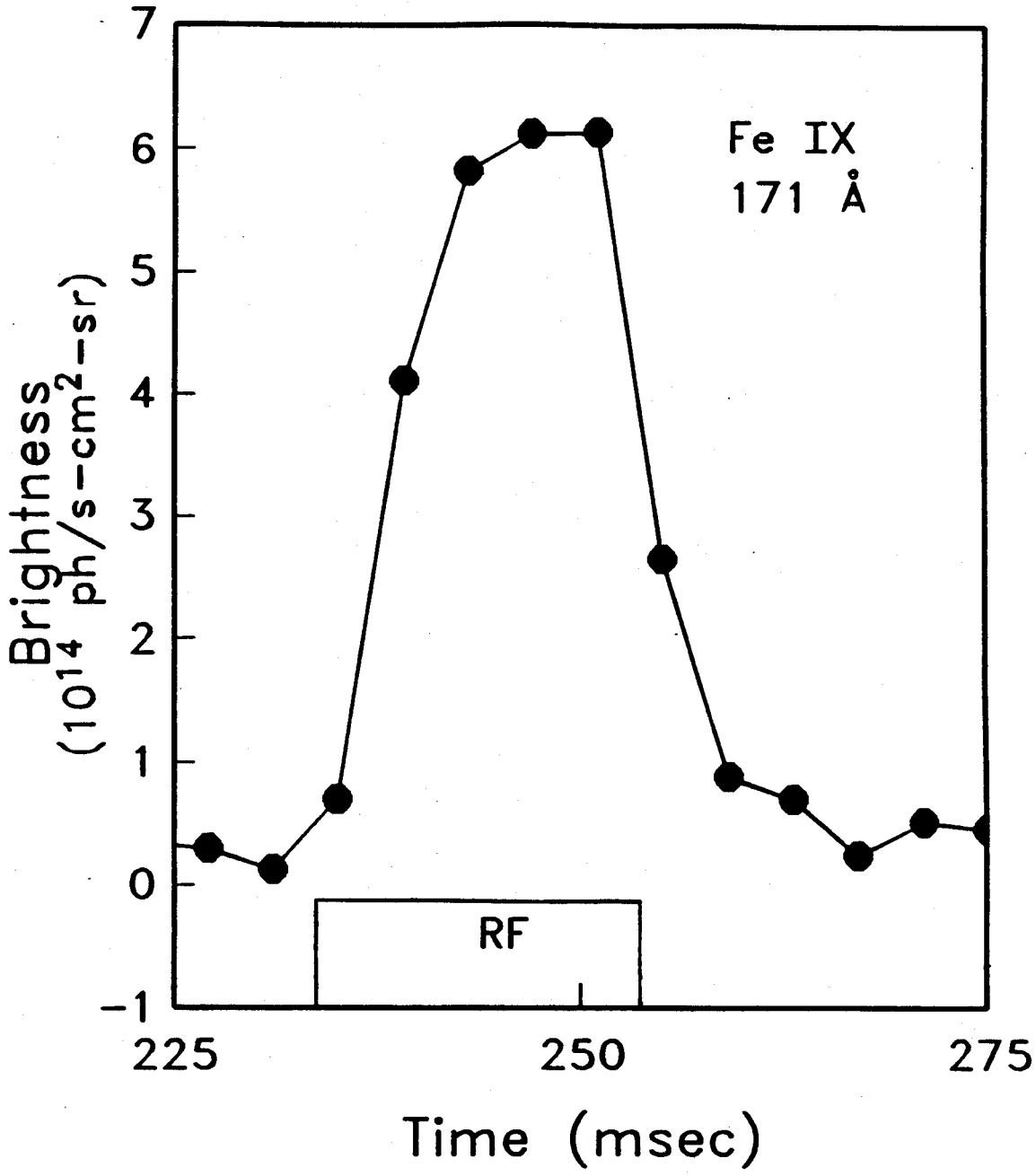


**Figure 4.** Evolution of the brightness of the Fe IX resonance line (171.09 Å) during ICRF ($P_{RF} \approx 350$ kW, minority hydrogen regime).

signature of the impurity rise on Alcator C, however, more closely resembled a sudden and large incremental rise in impurity production, as discussed above.

The results presented here indicate that the most likely mechanism generating the enhanced impurity influx is physical sputtering. Questions as to which structures (limiters, antennas, or walls) are the main sources, and which particles (thermal or fast ions, impurity ions, or neutrals) are doing most of the sputtering, and under what conditions this process is most pronounced (scalings) are addressed below.

The limiter, being in close contact with the plasma, is always suspect when impurity levels rise. Graphite limiters are known to become contaminated with surface deposits of metals after a period of exposure to tokamak plasmas with metal impurities [4,39,40]. Subsequent to the ICRF experiments, a graphite block from one of the Alcator C limiters was analyzed for surface composition via proton induced X-ray emission (PIXE), using 4.5 MeV protons. The results, shown in Figure 5, revealed metal deposits with iron surface concentrations as high as $2.4\times10^{17}$ atoms/cm$^2$, corresponding to an average thickness of roughly 100 monolayers. Also detected were smaller concentrations of molybdenum, chromium, nickel, and vanadium (believed to be an intrinsic impurity in the graphite). The impurity deposition profiles are peaked at the sides of the limiter, with minima at the center, where the plasma flux is tangent to the surface. This effect has been seen in previous studies of other tokamak limiters [41].

The contaminated limiters are believed to be the dominant source of metal impurities during the ohmic phase of the discharge. Results from the initial operations of JET indicated that contaminated graphite limiters were in fact the dominant source of metal impurities during ohmic discharges, even though Auger spectroscopy revealed the limiter surface still to be $\sim$ 90% carbon [42,43]. Although the metal concentrations observed on the Alcator C limiters are sufficient to allow for the amount of metallic impurity influx seen during ICRF heating pulses, it is very difficult to reconcile the dramatic increase in iron with the small change in carbon influx if the limiters are the source for both. No reasonable combination of changes in $T_e(r = a)$ and $n_e(r = a)$ could produce this effect in the erosion code simulations described below. This indicates that the main iron source during the RF pulse was *not* the contaminated limiters, but some other structure (the antenna Faraday shield, as seen below).

Still another argument concerns the presence of vanadium revealed by the PIXE analysis of the limiter block surface (Figure 5). Believed to be an intrinsic impurity in the graphite, it has a surface concentration only slightly less than that of nickel. While the resonance lines of highly ionized nickel become clearly visible during the RF pulse, similar lines from vanadium could not be detected. This implies that the limiters are not the main

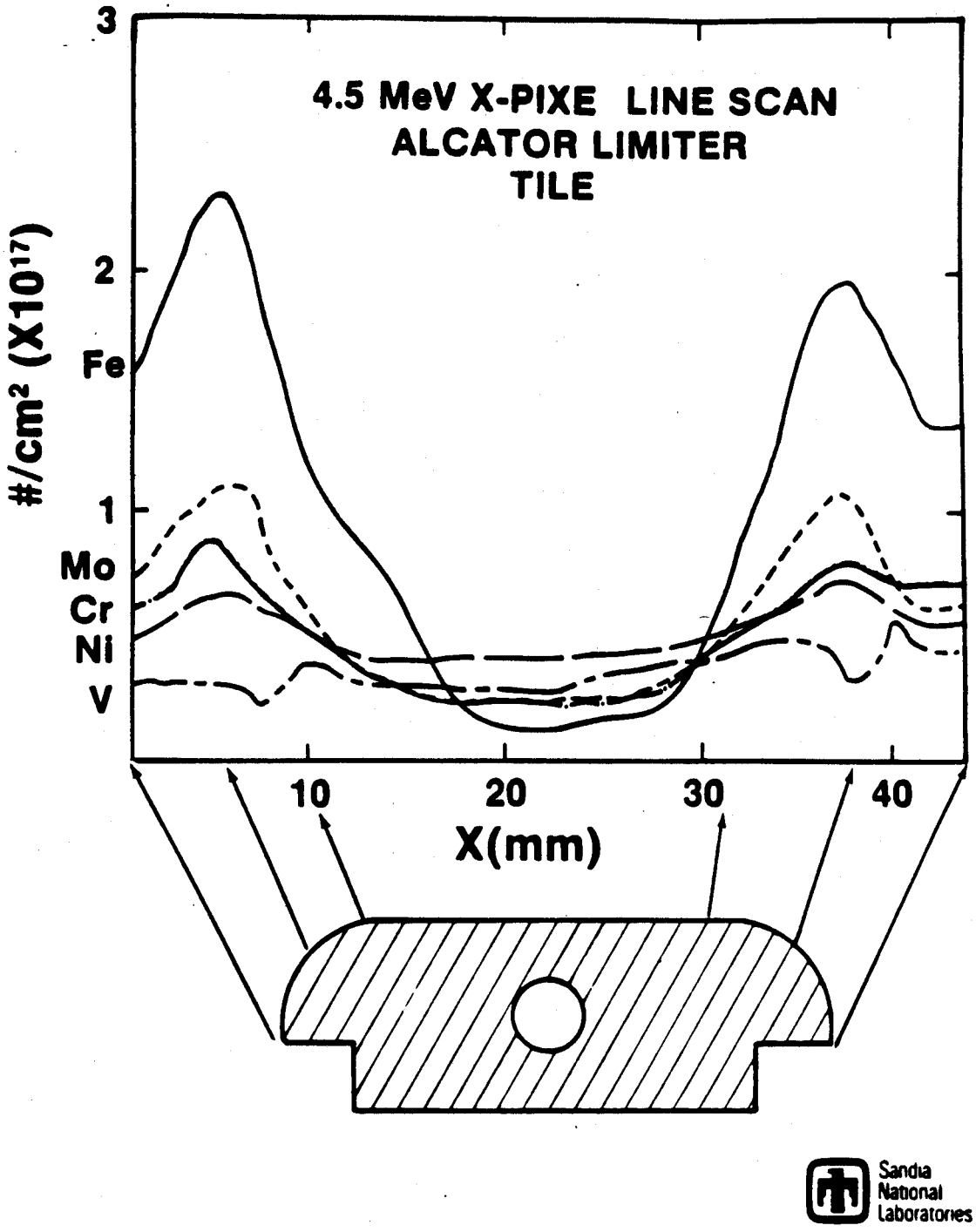


**Figure 5.** Surface concentrations of metal impurities on the graphite limiter tile. The X-axis is referenced to a cross-sectional view of the tile, looking in the poloidal direction.

source of nickel (or iron, etc.) during the RF pulse. However, an alternative explanation exists: since the PIXE analysis samples a layer a few microns thick, a relatively low concentration of vanadium, distributed uniformly throughout the sampled volume, could give the same signal as a high concentration of nickel, localized at the surface. In this case, the nickel would be much more susceptible to surface erosion processes during the RF pulse.

Other structures exposed to the edge plasma during these experiments include the stainless steel antenna Faraday shield at $r = 13.2$ cm, stainless supports for the graphite limiter blocks (exposed for $r \geq 14.5$ cm), secondary molybdenum limiters at 16.5 cm, stainless virtual limiters at 18.0 cm, and the stainless bellows wall at 19.2 cm.

In order to gain insight into the impurity production mechanism, the scaling of the iron influx with various plasma and RF parameters was studied. For a limited group of similar discharges with comparable RF pulse lengths, the change in iron influx, $\Delta\ S_{\rm Fe}$, may be taken to be proportional to the change in brightness, $\Delta B$, of an iron line from a non-central ionization state. However, the variety of plasma parameters employed in these experiments led to such a broad range of temperature profiles, density profiles, and transport conditions, that in general such a simple comparison of line brightnesses could be misleading. The transport code was therefore run for each set of plasma parameters used in order to arrive at a pre-RF value and an RF value for the iron influx in each discharge. The change in influx,

$$\Delta\ S_{\rm Fe} = S_{\rm Fe}^{RF} - S_{\rm Fe}^{Pre\ RF} \tag{3}$$

was then used to compare the impurity production due to ICRF power launched into different discharges. By bringing in transport parameters, this approach introduces additional quantitative uncertainties which may mask subtle dependences. For this survey, the following bright lines were used to deduce $S_{\rm Fe}$: a) the Fe-XVI resonance line ($3s - 3p$) at 335.407 Å, b) the Fe-XXIII resonance line ($2s^2 - 2s2p$) at 132.87 Å and the nearby Fe-XXII line ($2s^2 2p - 2s2p^2$) at 135.78 Å, and c) Fe-XXIV resonance line ($2s - 2p$) at 192.02 Å. Many other lines were viewed, of course, but these were chosen for the database study due to the amount of data on each and the quality of the atomic data (oscillator strengths and branching ratios) for the resonance lines.

The main conclusion of this survey is that the change in source rate during the injection of RF power, $\Delta S_{\rm Fe}$, increases with $P_{\rm RF}$ in a fashion that is approximately linear. This is especially evident in Figure 6a, in which only data points from a restricted group of shots with similar plasma parameters are plotted. In this case, as discussed above, the trend would be clear from simply plotting $\Delta B$ for a given iron line. For the larger,

unrestricted data set shown in Figure 6b, the values for a given $P_{RF}$ have been averaged, and the error bars indicate statistical variations of the individual points. Within the scatter, no clear dependence is seen on working gas, resonance conditions, or bulk plasma properties (with the exception of $\overline{n_e}$ at low densities, described below).

Absolute source rates are uncertain due primarily to uncertainties related to impurity transport in the peripheral plasma ($r > 0.75a$). For example, increasing the diffusion coefficient in this region by a factor of three leads to source rates ~four times higher. In addition, the presence of a non-zero inward convection term, $V(r) = V_o r/a$, in the impurity flux (Eqn. 1), can significantly influence the value of the deduced source rates. An examination of predicted vs. measured brightnesses for emission lines from a range of iron ionization states, each peaked at a different plasma radius due to the temperature profile, yields information about the total iron density profile, $n_{Fe}(r)$, which has a strong dependence on $V_o/D$. From such an examination it was concluded that the assumption $V_o = 0$, used in the calculations of source terms, was reasonable, and that an upper limit of $V_o < 2D/a$ could be established. Including this maximum value of $V_o$ in the transport code yielded iron source terms approximately 2.5 times smaller than those for which $V_o = 0$. Lines used for this profile study, and for calculating the average iron densities given in Table 1, were Fe-IX (171 Å), Fe-X (177 Å), Fe-XII (364 Å), Fe-XIII (368 Å), Fe-XIV (274 Å), Fe-XV (284 Å), Fe-XVI (336 Å), Fe-XVIII (94 Å), Fe-XIX (108 Å), Fe-XX (122 Å), Fe-XXI (142 Å), Fe-XXII (136 Å), Fe-XXIII (133 Å), and Fe-XXIV (192 Å). Hence, the uncertainties in the absolute source rates are estimated to be ± a factor of 3. Despite these uncertainties in the absolute rates, the relative changes are believed to be much more reliable and should allow determination of the major trends.

There is no correlation of $\Delta S_{Fe}$ with the fast ion distribution as inferred from the perpendicular neutral particle flux in the energy range $.9 < E < 10.$ keV due to CX. This is the case whether or not the observed flux comes from the plasma edge or the plasma center. In fact, the CX flux in this energy range typically decreases during ICRF injection. Thus, it is inferred that the impurity production is unrelated to the presence of fast ion tail formation or to a change in $T_i$ due to ICRF heating. However, it must be emphasized that the CX neutral analyzer did not detect particles with $E < 900$ eV, and it did not measure parallel distributions. The flux below 2 keV comes predominantly from the outer plasma region in Alcator C. Furthermore, the CX analyzer was not at the same toroidal location as the ICRF antenna, and would therefore probably not detect any local production of fast, promptly lost ions. However, if the increase in molybdenum (see Figure 3 and Table I) results from erosion of the secondary molybdenum limiters at 16.5 cm, as suspected, then localized erosion near the antenna would not be indicated.

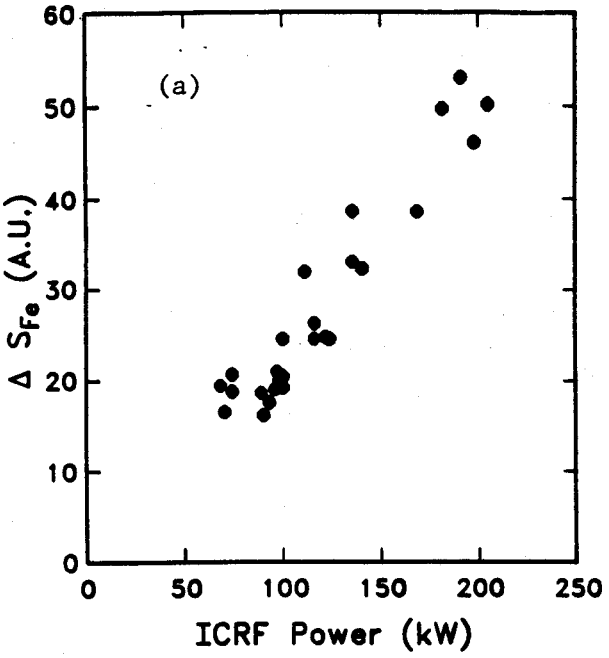


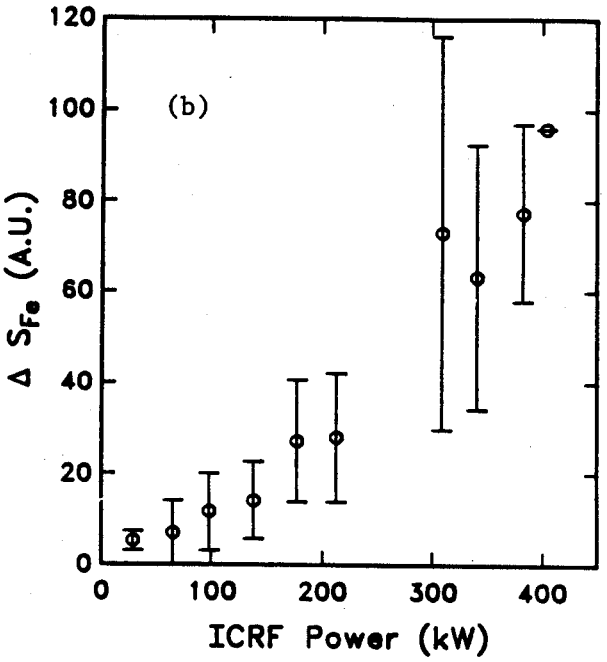


**Figure 6.** Change in iron source rate, $\Delta S_{Fe}$, vs. injected RF power. (a): Individual data points from a restricted set of similar plasma discharges (H 2nd harmonic regime only; all points derived from Fe-XXIII resonance line at 132.87 Å). (b): Average values for all the data. Error bars represent statistical variations from the average.

The lower half-loop antenna was installed first and operated alone for the first three weeks. Upon the installation of the upper half-loop, the antennas were usually operated together, with the RF power being split roughly equally between them. At times, however, each half-loop was also operated individually. For all cases, the iron influx was approximately the same for a given total $P_{RF}$ , indicating no strong dependence on either antenna poloidal extent or on the total exposed antenna area (activated or not). However, the scatter in the data could mask the factor of 2 changes one might have expected.

Two conditions associated with elevated edge temperatures are correlated with enhanced impurity production: low density and low limiter safety factor, $q$. Below a threshold value of $\overline{n_e} \approx 1.8 \times 10^{14}$ cm$^{-3}$, $\Delta S_{Fe}$ is seen to increase as $\overline{n_e}$ decreases. The probable explanation for this result involves the deterioration of energy confinement times on Alcator C at lower values of $\overline{n_e}$ (Alcator scaling) [44]. The edge temperature $T_{eb}$ generally increases as $\overline{n_e}$ decreases past a certain value, which would lead to increased sputtering losses. This mechanism has been suggested previously to explain high metal concentrations during low density ohmic discharges on Alcator C [45]. Furthermore, $\Delta S_{Fe}$ is often higher for lower $q$ discharges with $q_l \leq 3.4$, another condition associated with elevated edge temperatures.

Further corroboration of this effect is seen from the Langmuir probe data, which yielded strong evidence for a prompt and large change in $T_{eb}(r)$ at the antenna radius during the RF pulse (Figure 7).

The values of $T_{eb}$ deduced during the ICRF pulse may actually be regarded as a lower limit on the electron temperature, as the probe I-V characteristic was limited by the bias sweep voltage employed during these experiments. If there were, for example, a fast electron component ($T_{eb} > 40$ eV) present in addition to a slower component, the deduced temperature would correspond to the colder component of the distribution. However, no clear evidence for such a tail was seen in these experiments. Also, more recent measurements made by a gridded energy analyzer in the SOL during ICRF heating experiments have shown the distributions of electrons and ions with energy $E \lesssim 70$ eV to be well described by thermal distributions whose temperatures increase during the RF pulse [46].

Only minor changes in $n_{eb}(r)$ were seen. Plotted in Figure 8 are the iron source terms before and during the RF pulse ($S_{Fe}^{Pre\ RF}$ and $S_{Fe}^{RF}$) versus $T_{eb}$ at the antenna radius, for a series of shots with $P_{RF}$ in the 50 kW range, showing a clear correlation. The increase, if any, in $T_{eb}(r)$ at the limiter radius was less dramatic, leading to an effective increase in the edge temperature scrape off length by a factor of three or more during the 350 kW RF pulses. A similar flattening of the edge temperature profile has been reported at TEXTOR [6] and at JET [5]. Since the Langmuir probe was located toroidally away

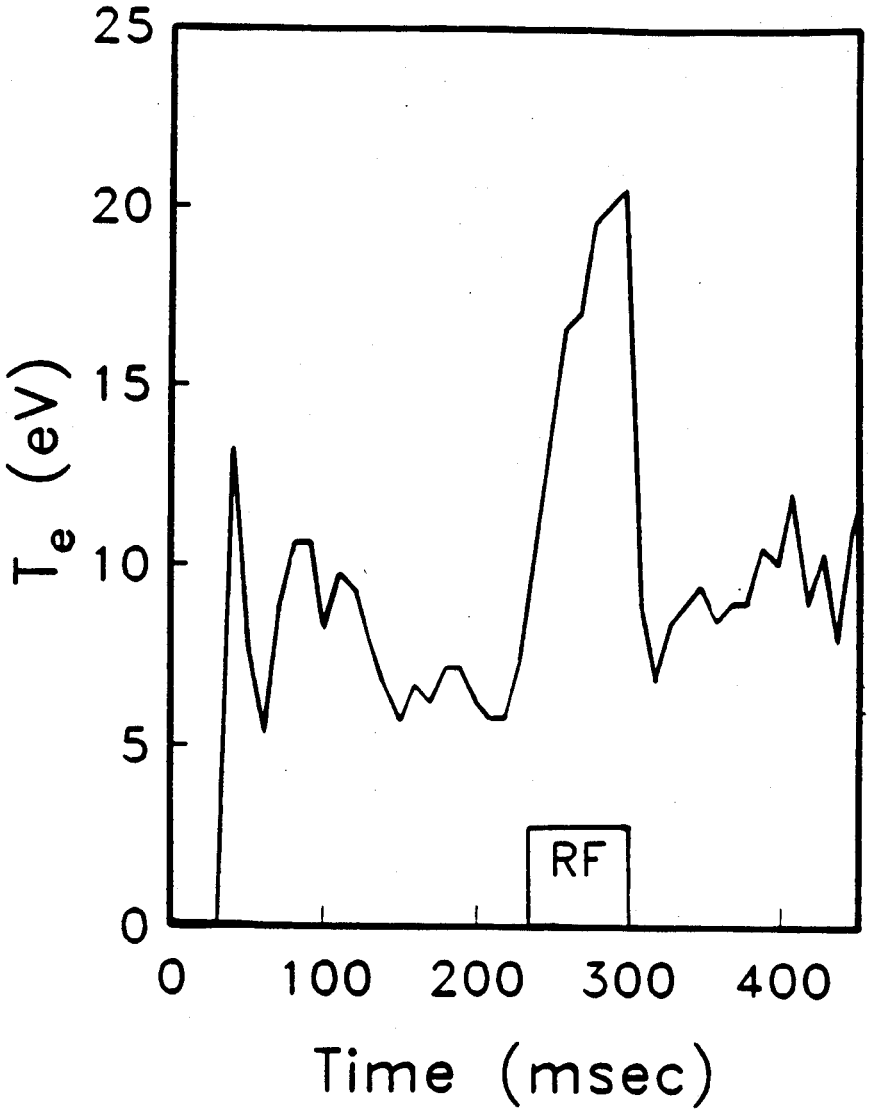


**Figure 7.** Evolution of boundary electron temperature $T_{eb}$, measured by a Langmuir probe at the antenna radius, during a 380 kW ICRF pulse.

from the antenna, this change in the edge plasma was not a local effect. Of course, the perturbation may have been larger at the antenna port.

The above evidence strongly suggested that thermal sputtering of the Faraday shield through a significantly increased sheath potential ($\Phi_{sh} \approx 3T_{eb}$) was the dominant source of iron, chromium, and nickel during the ICRF pulse. An increase in $T_{eb}$ from 6 eV to 20 eV at the antenna, as shown in Figure 7, would cause the sputtering of iron by protons to increase by an order of magnitude due to the sharp increase in sputtering coefficient with increasing impact energy [37]. If for some reason a fast electron component is created in the SOL during the RF pulse, corresponding to a higher temperature than that deduced from the Langmuir probe data, then the sheath potential would undergo an even larger increase. The more modest changes in the carbon and oxygen influx are ascribed to the more modest increases in $T_{eb}$ at the limiter, again via thermal sputtering. Sputtering contributions from the limiter supports and wall are estimated to be minor because they are $\sim$ 7 and 22 density scrape-off lengths behind the limiter, respectively. Coupled with the observed lack of dependence on CX neutral flux, this tends to eliminate these structures from consideration.

An observation from the current (1985-86) ICRF heating experiments on Alcator C supports the identification of the Faraday shield as the primary metal source during ICRF heating. Visible light emission from the antenna region was seen to increase during the RF pulse, and in fact it closely tracked the time dependence of $P_{RF}$ . A filter transparent to $H_\alpha$ radiation cuts off this light, implying that it is not due to hydrogen or deuterium. Rather, the emission is believed to be radiated from neutral or lightly ionized metal atoms entering the plasma.

Sputtering yields are predicted to be roughly a factor of $\sqrt{2}$ higher for deuterium than for hydrogen, an effect which is either not seen or obscured by the scatter in the data. This scatter is attributed largely to small changes in the edge plasma parameters. The Langmuir probe was available for only a few days during these experiments, so only limited comparisons of impurity influx with edge parameters (such as in Figure 8) are possible.

## 5. Erosion code comparison

To quantitatively check the validity of the above conclusions, an edge erosion code was used to calculate heating, evaporation/sublimation rates, and thermal sputtering rates. Using edge plasma parameters and the physical properties of the exposed structural materials as input, the code yields calculated impurity source rates from both the limiter and Faraday shield [47]. The overall sputtering yield includes thermal sputtering by bulk ions (H or D) and self-consistent contributions from impurity ions. Edge profiles $T_{eb}(r)$ and

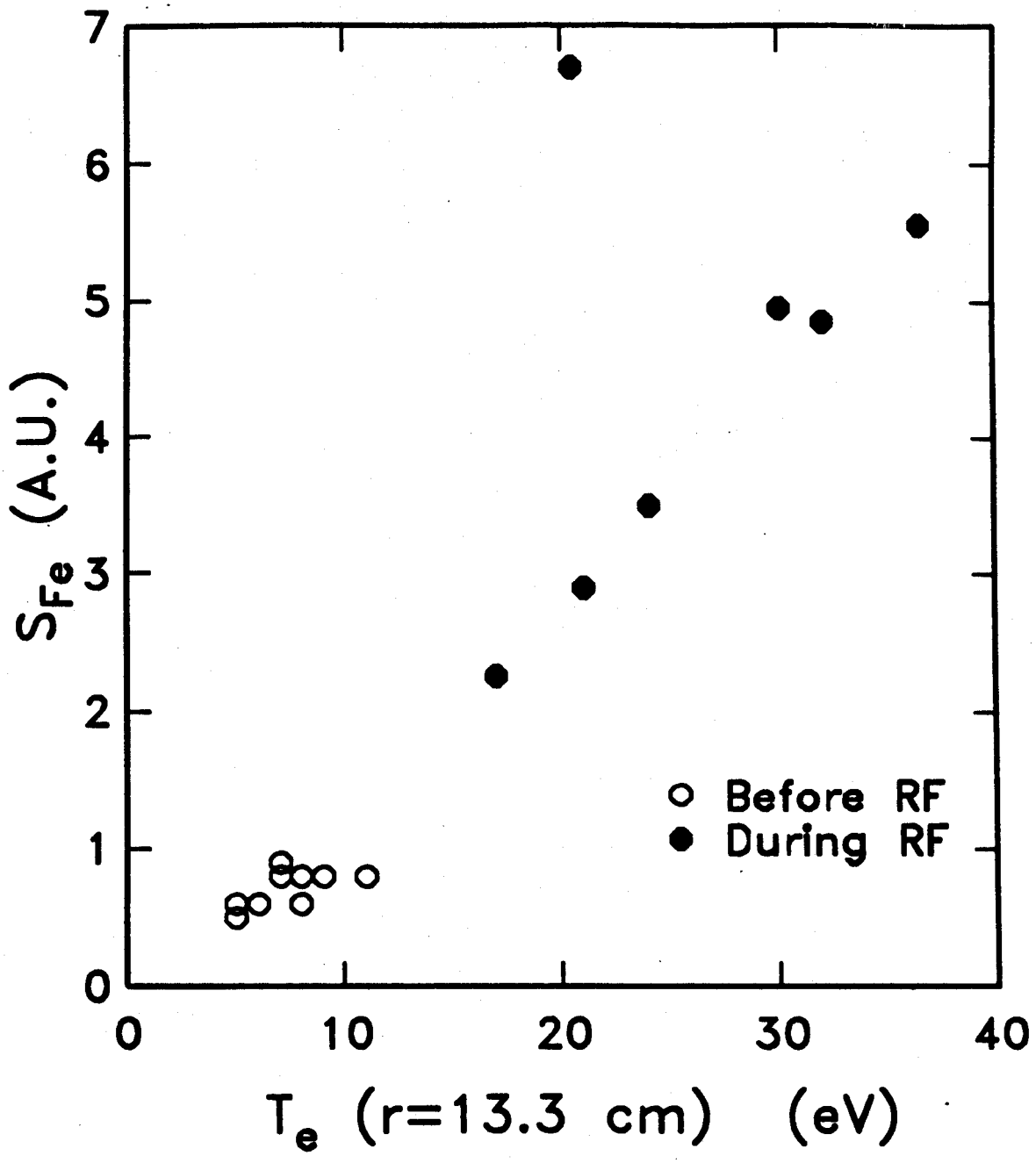


**Figure 8.** Iron source rate $S_{Fe}$ before and during the RF pulse, plotted vs. $T_{eb}$ at the antenna radius for similar shots with $P_{RF} \approx 50$ kW, hydrogen, $B_T \approx 8$ T (non-resonant).

$n_{eb}(r)$ consistent with values measured by the Langmuir probe during a series of 350 kW ICRF discharges were used in order to compare calculated iron and carbon source rates with those inferred from the data in Table I. The edge temperature profile $T_{eb}(r)$ was assumed to change rapidly from pre-RF to RF conditions. Edge ion temperatures, $T_{ib}(r)$, were taken to be three times $T_{eb}(r)$, consistent with recent edge measurements on Alcator C [46]. Note that for ion sputtering, the impact energy $E \sim T_{ib} + Z_i \Phi_{\mathbf{sh}}$.

By adjusting the edge plasma parameters within the experimental uncertainties, excellent qualitative and reasonable quantitative agreement could be obtained (Figure 9). In this calculation, thermal sputtering by deuterons accounts for almost half the iron and carbon influx, with the remainder due to impurity ion sputtering. The contributions from evaporation and sublimation are much too small to explain the observed influxes. As stated earlier, no conditions could be found to produce the observed influxes of both carbon and iron solely from the contaminated graphite limiter.

While the agreement between the erosion code and the observed impurity behavior strongly supports the conclusion that thermal sputtering is the dominant mechanism generating the impurities, it cannot be construed as a proof which eliminates other possible mechanisms. There are significant uncertainties in the detailed plasma profiles in the scrape off layer, as well as uncertainties in the impurity transport in the plasma periphery (from $r > .75a$ to the wall). It should be noted that the total power flux to the limiters can be calculated from the edge profiles used in the erosion code. For the edge values giving the reasonable match shown in Figure 9, the calculated power to the limiters is $\sim 50\%$ higher than the total input power minus the radiated power. Edge values giving better agreement in the scraped off power reduce the predicted source rates by factors of ~2–3, but these are still within the uncertainties of the source rates implied by the spectroscopic measurements and transport analysis. In addition, the effects of possible toroidal or poloidal asymmetries in the edge are not included in the calculations. In particular, the temperature and density near the antenna during the RF pulse might differ considerably from the values recorded by the Langmuir probe and modeled in the erosion code. Hence the reasonably good agreement shown in Figure 9 gives significant credibility to the impurity production model, but it can not be used to rule out those processes which are difficult to model, such as unipolar arcing or sputtering due to reactive $\vec{E}_{RF}$ fields.

## 6. Discussion

The picture which emerges from the above analysis is one of elevated edge temperatures in the SOL during ICRF, which in turn lead to an enhanced impurity influx due to physical sputtering through an elevated sheath potential. Because the relative increase in

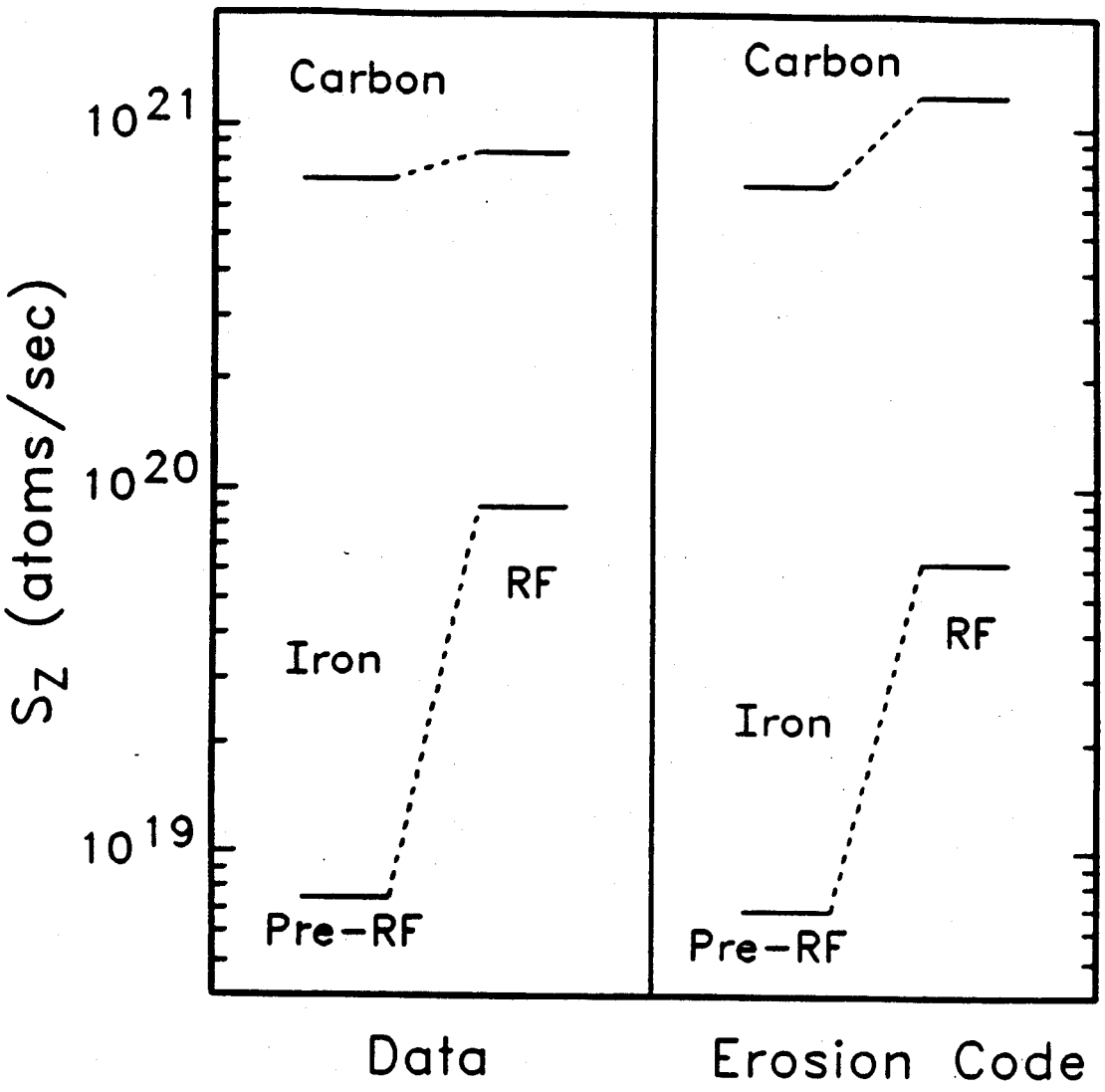


**Figure 9.** Comparison of the iron and carbon source rates deduced from the spectroscopic data with the rates calculated by the erosion code. Levels are shown for before and during the ICRF pulse under conditions similar to those of Fig. 1.

edge temperature is larger at the radius of the antenna than at the radius of the limiter, the largest percent increase in impurity influx is that for the materials in the antenna shield (chiefly iron, chromium, and nickel). This explanation of enhanced impurity production in Alcator C during ICRF heating is consistent with both experimental evidence and results from other tokamaks. Thermal sputtering due to elevated $T_{eb}$ during ICRF was also blamed for enhanced metallic impurity levels at T-10 [48] and at TFR [15-18], where the results and conclusions are generally similar to those reported here for Alcator C. This process is also blamed for enhanced sputtering of C and O from the graphite limiter of JFT-2M. The rise in $T_{eb}$ is also seen in JIPP T-IIU. Although $T_{eb}$ was not reported to rise on PLT, it is stated that noise on the probe signals could have prevented the detection of such an effect.

However, this picture does not explain how the ICRF power changes the edge plasma. The fact that both the impurity influx and $T_{eb}$ change quickly upon turning on the RF power implies that the change is due to some direct heating of the edge plasma from the antenna, rather than to increased energy flux out of the central plasma, (which often showed little change in $T_e$ or $T_i$ anyway). This edge heating appears to be relatively insensitive to how well the launched ICRF power propagated and was absorbed by the bulk plasma, as evidenced by the lack of correlation with resonance conditions. Possible edge heating processes include the damping of coaxial modes or surface waves [49], excitation and damping of the slow wave in the SOL [22], or absorption at the lower hybrid resonance layer, which occurs in the SOL at $n_i \approx 10^{12}$ cm$^{-3}$ for these experiments. The scaling with $P_{RF}$ may indicate that some constant fraction of the launched ICRF power goes directly into the edge plasma. To raise the temperature of the low density plasma in the SOL by 20 ev or so would require less than 2% of the 400 kW delivered to the antenna for the shots with the highest power, assuming an energy confinement time of 0.5 ms in the SOL. The possibility of a local maximum in $T_{eb}(r)$ at the radius of the antenna would require that the power was absorbed in a fairly narrow radial zone. Indeed, some indication of such a profile has been seen in the more recent Alcator C ICRF experiments [46].

Increased sputtering from CX neutrals was invoked by JIPP T-IIU workers to explain increased O levels, and metal influx on JFT-2 during ICRF was correlated with fast ions in the edge. At PLT, sputtering calculations showed that an elevated efflux of both low energy ($E \leq 1$ keV) and fast neutrals, measured during ICRF, was sufficient to account for the observed influx of iron from the stainless steel walls [2,12]. Highly energetic trapped ions, detected in the SOL of PLT during ICRF [50], may also play a role. No such correlation with fast ions or neutrals ($E > 900$ eV), was observed on Alcator C, although local effects near the antenna cannot be completely dismissed. The lack of a low energy neutral analyzer

prevented any such study of ions having $E \leq 900$ eV.

Sputtering of the antenna Faraday shield and walls due to the acceleration of ions by the reactive $\vec{E}_{RF}$ fields near the antenna was blamed for metallic impurity generation at JFT-2M and Macrotor [51] during ICRF. To examine this possibility on Alcator C, calculations based on the formulas of Itoh *et al.* [52] were performed to estimate the impact energy with which ions accelerated by the $\vec{E}_{RF}$ fields would strike the Faraday shield. The electric field was estimated to be $\lesssim$ 1000 V/cm near the Faraday shield, resulting in impact energies generally too small ($E \leq 10$ eV) to cause much sputtering. An exception is the case of minority hydrogen ions in a magnetic field of $\vec{B} = 12$ Tesla, for which the fundamental cyclotron resonance layer of hydrogen occurs on axis. The lack of observed dependence of impurity influx on magnetic field or working gas, coupled with the low impact energy predicted under most conditions, indicates that this process is not a dominant source of iron on Alcator C.

The occurrence of a large number of small unipolar arcs between the Faraday shield and the plasma sheath, yielding an iron source which increases with $P_{RF}$ , also cannot be ruled out. However, the arc tracks would have had to be so small that they were not identifiable upon visual inspection of the antenna. The Alcator C results are consistent with the conclusion, also reached at PLT [10] and JIPP T-IIU [26], that the closest metal surface to the plasma, if unprotected, will yield the largest metal impurity influx. Thus the unprotected antenna Faraday shield on Alcator C is the probable dominant source of iron, chromium, and nickel during ICRF despite metallic contamination of the graphite limiter.

The use of graphite protective shields on the antenna surfaces which intercept magnetic flux lines, as employed at TFR and PLT, apparently minimizes the antenna contribution to the metallic impurity influx. Good ICRF heating results at $P_{RF} \leq$4.5 MW have also been recently reported at JET [5,53] which uses graphite protective tiles around the antenna in conjunction with carbonization of the walls to reduce metal impurity production. Despite a flattening of the SOL profiles which yields a modest rise in the edge temperature during ICRF heating and some increase in density near the wall, the level of nickel (dominant metal impurity) in the plasma rises no faster than the total input power, and does not play a dominant role in the central power balance. The price for such success, however, is substantial amounts of carbon in the plasma. Carbonization of the walls has also been recently reported to be effective for the attainment of long-pulse ($\sim$ 1 sec), high power ($\sim$ 2.25 MW) ICRF heating at TEXTOR with negligible metal influx [6]. Tests with a movable steel plate indicated that metal erosion in the SOL was due to sputtering by ions, perhaps involving a postulated suprathermal component. Prior to the carboniza-

tion, the TEXTOR edge plasma and SOL were strongly perturbed by the ICRF pulse, and impurity problems limited the RF pulse to 200 kW for 100 msec. Similar success using wall carbonization to overcome enhanced impurity levels during ICRF heating has also been recently reported at the diverted tokamak ASDEX (2.3 MW, 1 sec ICRF), [7].

The effects of ICRF heating on $n_{eb}$ have varied from one experiment to the next. These effects are generally attributed to changes in desorption and recycling at the wall and may depend on details of the limiter-antenna-wall spacings. Neither large nor reproducible effects were seen on Alcator C, where the distance from the wall to the front of the ICRF antenna is $\sim 6.0$ cm, or $\sim 20$ times the density scrape-off length.

## 7. Summary

The following conclusions have been drawn from the analysis of spectroscopic and other data taken during ICRF heating experiments on Alcator C:

(a) Large increases in metallic impurity concentrations were observed (factor of $\sim 12$ for 400 kW RF). Smaller increases were seen in the light impurities (factor of $\sim 1.2$ for carbon and $\sim 1.9$ for oxygen). Graphite limiters and stainless steel Faraday shields were used during these experiments.

(b) The change in deduced iron influx, $\Delta S_{\mathrm{Fe}}$, increases approximately linearly with $P_{\mathrm{RF}}$ for a variety of plasma and RF conditions.

(c) A prompt increase in $T_{eb}$ at the antenna radius is seen during the ICRF pulse. The magnitude of this increase correlates well with $\Delta S_{\mathrm{Fe}}$.

(d) No correlation of $\Delta S_{\mathrm{Fe}}$ is detected with working gas, plasma conditions, heating mode, antenna area exposed or activated, bulk ion heating, ion tail formation, or fast neutral particle flux.

(e) It is concluded that physical sputtering of the stainless steel antenna Faraday shield due to an elevated sheath potential ($\Phi_{\mathrm{sh}} \approx 3T_{eb}$) is the primary source of metallic impurities during ICRF heating on Alcator C. The same process, occurring at the graphite limiter, is believed to be the dominant source of carbon and oxygen. Modeling suggests that the sputtering is due both to working gas and impurity ions.

(f) These conclusions are consistent with calculated sputtering yields obtained from an edge erosion code which utilized the measured changes in edge temperature profiles. The code predicts negligible contributions from evaporation and sublimation, and strongly discredits the possibility of the contaminated limiter being the dominant source of metal impurities during ICRF.

To unravel further the effects of ICRF heating on impurity production, it is desirable to monitor closely the edge plasma conditions, both globally and near the antenna struc-

ture. An investigation into the possible mechanisms for direct deposition of RF energy into the SOL plasma would also help antenna designers minimize this process, which appears to be closely tied to impurity generation.

**Acknowledgements:**

The rest of the Alcator C research and support staff are thanked for their help in operating the tokamak and taking data. We also thank Dr. Barney Doyle of Sandia Laboratory for the PIXE analysis of the graphite limiter block. This work was carried out under United States Department of Energy contract no. DE-AC02-78ET51013.

## References


1. Swanson, D.G. *Phys. Fluids* **28** (1985) 2645.

2. Cohen, S.A., Bernabei, S., Budny, R., Chu, T.K., Colestock, P., *et al.*, *J. Nucl. Materials* **128-9** (1984) 280.

3. TFR Group, Sand, F., *Nucl. Fus.* **25** (1985) 1719.

4. Staudenmaier, G., *J. Vac. Sci. Technol. A* **3** (1985), 1091.

5. Jacquinot, J., Anderson, R.J., Arbez, J., Bartlett, D., Beaumont, B., *et al.*, *Plasma Phys. and Cont. Fus.* **28** (1986) 1. See also a) Englehardt, W., *et al.*, " Impurity Behavior in JET", and b) Brinkschulte, H., Tagle, J.A., Bures, M., Erents, S.K., Harbour, P., *et al.*, " Behaviour of Plasma Boundary During ICRF in JET", both in *Proc. Euro. Phys. Soc. Conf. on Plasma Phys. and Cont. Fusion*, Schliersee, 1986 (to be published).

6. Messiaen, A.M., Bhatnagar, V.P., Delvigne, T., Descamps, P., Durodié, F., *et al.*, *Plasma Phys. and Contr. Fus.* **28** (1986) 71. See also Schweer, B., Bay, H.L., Bieger, W., Bogen P., Hartwig, H., *et al.*, in *Proc. Euro. Phys. Soc. Conf. on Plasma Phys. and Cont. Fusion*, Schliersee, 1986 (to be published).

7. Steinmetz, K., Fußmann, G., Gruber, O., Niedermeyer, H., Müller, E.-R., *et al.*, *Plasma Phys. and Contr. Fus.* **28** (1986) 235. See also Janeschitz, G., Fussmann, G., Steinmetz, K., ASDEX-, NI-, and ICRH- Teams, "Impurity Production During ICRF Heating", in *Proc. Euro. Phys. Soc. Conf. on Plasma Phys. and Cont. Fusion*, Schliersee, 1986 (to be published).

8. Weynants, R.R., in *Heating in Toroidal Plasmas*, (Proc. 4th Intl. Sympos., Rome, 1984), Vol.I, Intl. School of Plasma Physics, Varenna (1984) 211.

9. Suckewer,S., Hinnov, E., Hwang, D., Schivell, J., Schmidt, G.L., *et al.*, *Nuclear Fusion* **21**, (1981) 981.

10. Hosea, J., Bell, R., Budny, R., Cavallo, Cohen, S., *et al.*, in *Heating in Toroidal Plasmas*, (Proc. 4th Intl. Sympos., Rome, 1984), Vol.I, Intl. School of Plasma Physics, Varenna (1984) 261.

11. Stratton, B.C., Moos, H.W., Hodge, W.L., Suckewer, S., Hosea, J.C., *et al.*, *Nucl. Fus.* **24** (1984), 767.

12. Cohen, S.A., Ruzic, D., Voss, D.E., Budny, R., Colestock, P., *et al.*, *Nucl. Fus.* **24** (1984), 1490.

13. Equipe TFR, in *Heating in Toroidal Plasmas*, (Proc. 3rd Joint Varenna-Granoble Intl. Sympos., Grenoble, 1982), Vol. III, Commission of the European Communities, Brussels (1982) 1177.

14. TFR Group, in *Radiation in Plasmas*, Vol. 1, ed. by M. McNamara (Reviews of 1983 College on Plasma Physics, Trieste, Italy), 259.

15. TFR Group, in *Proc. 11th European Conf. on Cont. Fusion and Plasma Physics, Aachen* (1983), Europhysics Conf. Abstracts, Vol. 7D, European Phys. Soc., Geneva (1983) 493.

16. Equipe TFR, *Plasma Physics and Controlled Fusion* **26** (1984) 165.

17. Equipe TFR, in *Heating in Toroidal Plasmas*, (Proc. 4th Intl. Sympos., Rome, 1984), Vol.I, Intl. School of Plasma Physics, Varenna (1984) 277.

18. TFR Group, *J. Nucl. Materials* **128-9** (1984) 292.

19. Breton, C., De Michelis, C., Hecq, W., Mattioli, M. Ramette, J., Saoutic, B.,*Plasma Physics and Cont. Fusion* **27** (1985), 355.

20. JFT-2 Group, in *Heating in Toroidal Plasmas*, (Proc. 3rd Joint Varenna-Granoble Intl. Sympos., Grenoble, 1982), Vol. III, Commission of the European Communities, Brussels (1982) 1191.

21. JFT-2 Group, in *Heating in Toroidal Plasmas*, (Proc. 3rd Joint Varenna-Granoble Intl. Sympos., Grenoble, 1982), Vol. I, Commission of the European Communities, Brussels (1982) 259.

22. Kimura, H., Matsumoto, H., Odajima, K., Konoshima, S., Yamamoto, T., *et al.*, in *Plasma Physics and Controlled Nuclear Fusion Research*, Proc. 9th Int. Conf. Baltimore 1982), Vol.2, IAEA, Vienna (1983) 113.

23. Ogawa, H., Odajima, K., Ohtsuka, H., Matsumoto, H., Kimura, H., *et al.*, *J. Nucl. Materials* **128-9** (1984) 298.

24. Odajima, K., Matsumoto, H., Kimura, H., Hoshino, K., Kasai, S., *et al.*, in *Heating in Toroidal Plasmas*, (Proc. 4th Intl. Sympos., Rome, 1984), Vol.I, Intl. School of Plasma Physics, Varenna (1984) 243.

25. Ichimura, M., Fujita, J., Hirokura, S., Kako, E., Kawahata, K., *et al.*, ICRF Heating Experiments on JIPP T-II, Nagoya Univ., Inst. of Plasma Physics, Rep. IPPJ-650 (1983).

26. Noda, N., Watari, T., Toi, K., Kako, E., Sato, K., *et al.*, *J. Nucl. Mat.* **128-9** (1984) 304.

27. Toi, K., Watari, T. Ohkubo, K., Kawahata, K., Noda, N., *et al.*, in *Plasma Physics and Controlled Nuclear Fusion Research*, Proc. 10th Int. Conf. London, 1984), Vol.1, IAEA, Vienna (1985) 523.

28. Porkolab, M., Blackwell, B., Bonoli, P., Griffin, D., Knowlton, S., *et al.*, in *Plasma Physics and Controlled Nuclear Fusion Research*, Proc. 10th Int. Conf. London, 1984), Vol.1, IAEA, Vienna (1985) 463.

29. Blackwell, B.D., Moody, J.D., Parker, R.R., Porkolab, M., and the Alcator Group. *Bull. Amer. Phys. Soc.* **29** (1984) 1219.

30. Bell R.E., Finkenthal, M., Moos, H.W., *Rev. Sci. Instrum.* **52** (1981) 1806.

31. Fonck, R.J., Ramsey, A.T., Yelle, R.V., *Appl. Optics* **21** (1982) 2115.

32. Hodge, W.L., Stratton, B.C., Moos, H.W., *Rev. Sci. Instrum.* **55** (1984) 16.

33. Manning, H.L., Terry, J.L., Marmar, E.S. *Bull. Am. Phys. Soc.* **28** (1983), 1250.

34. TFR Group, *Nucl. Fus.* **25** (1985), 1767.

35. Marmar, E.S., Rice, J.E., Terry, J.L., Seguin, F.H., *Nucl. Fus.* **22** (1982), 1567.

36. Post, D.E., Jensen, R.V., Tartar, C.B., Grasberger, W.H., Lokke, W.A., *Atomic Data and Nucl. Data Tables* **20** (1977), 397.

37. McCracken, G.M., Stott, P.E., *Nucl. Fus.* **19** (1979), 889.

38. Demidenko, I.I., Leonov, V.M., Lomino, N.S., Ovcharenko, V.D., Padalka, V.G., Polyakova, G.N., *Sov. J. Plasma Phys.* **10** (1984) 292.

39. Ehrenberg, J., Behrisch, R., Surface Analysis of a Central Part of the JET Graphite Limiter, Max-Planck-Inst. für Plasmaphysik, Garching, Report IPP 9/47, (1984).

40. Behrisch, R., Børgesen, P., Ehrenberg, J., Scherzer, B.M.U., Sawicka, B.D. *et al.*. *J. Nucl. Materials* **128-9** (1984), 470.

41. Doyle, B., Sandia National Lab., Albuquerque, private communication (1985).

42. Behringer, K.H., Carolan, P.G., Denne, B., Decker, G., Engelhardt, W., *et al.*, Impurity and Radiation Studies During the JET Ohmic Heating Phase, JET Joint Undertaking, Abingdon, Report JET-P(85)08 (1985) (subm. to Nucl. Fusion).

43. Ehrenberg, J., Behrisch, R., Coad, J.P., Erents, K., De Kock, L., *et al.*, *Bull. Am. Phys. Soc.* **30** (1985), 1525.

44. Parker, R.R., Greenwald, M., Luckhardt, S.C., Marmar, E.S., Porkolab, M., Wolfe, S.M, *Nucl. Fus.* **25**, 1127 (1985).

45. Rice, J.E., Marmar, E.S., Lipschultz, B., Terry, J.L., *Nucl. Fusion* **24**, (1984) 329.

46. Wan, A., Plasma Fusion Center, Mass. Inst. of Tech., private communication (1985).

47. Lipschultz, B., LaBombard, B., Manning, H.L., Terry, J.L., Knowlton, S., *et al.*, Impurity Sources During Lower-Hybrid Heating on Alcator C, M.I.T. Plasma Fusion Center Report PFC/JA-85-45 (1985).

48. Vertiporokh, A., Kurchatov Inst., Moscow,private communication (1985).

49. Messiaen, A.M., Koch, R., Bhatnagar, V.P., Vandenplas, P.E., Weynants, R.R., in *Heating in Toroidal Plasmas*, (Proc. 4th Intl. Sympos., Rome, 1984), Vol.I, Intl. School of Plasma Physics, Varenna (1984) 315.

50. Manos, D.M., Stangeby, P.C., Budny, R.V., Cohen, S.A., Kilpatrick, S., Satake, T., *J. Nucl. Materials* **128-9** (1984) 319.

51. Taylor, R.J., Evans, J., Keller, L., Lai, K.F., Rossing, V., *et al.*, in *Plasma Physics and Controlled Nuclear Fusion Research*, (Proc. 10th Int. Conf. London, 1984), Vol.1, IAEA, Vienna (1985) 581.

52. Itoh, K., Fukuyama, A., Itoh, S., A Possible Origin of Metal Impurities in ICRF Heating Experiments, Hiroshima Univ., Inst. for Fusion Theory Report HIFT-93 (1984).

53. Erents, S.K., Stangeby, P.C., Tagle, J.A., McCracken, G.M., De Kock, L., Stott, P.E., *Bull. Am. Phys. Soc.* **30** (1985), 1525.